Creation of paired electron states in the gap of semiconducting carbon nanotubes by correlated hydrogen adsorption

Gilles Buchs[1,4]**, Arkady V Krasheninnikov**[2,3]**, Pascal Ruffieux**[1]**, Pierangelo Gröning**[1]**, Adam S Foster**[3]**, Risto M Nieminen**[3] **and Oliver Gröning**[1]

[1] EMPA Swiss Federal Laboratories for Materials Testing and Research, nanotech@surfaces, Feuerwerkerstrasse 39, CH-3602 Thun, Switzerland
[2] Accelerator Laboratory, University of Helsinki, P O Box 43, FI-00014, Finland
[3] Laboratory of Physics, Helsinki University of Technology, P O Box 1100, FI-02015, Finland
E-mail: gilles.buchs@empa.ch

Abstract. The specific, local modification of the electronic structure of carbon nanomaterials is as important for novel electronic device fabrication as the doping in the case of silicon-based electronics. Here, we report low temperature scanning tunneling microscopy and spectroscopy study of semiconducting carbon nanotubes subjected to hydrogen-plasma treatment. We show that plasma treatment mostly results in the creation of paired electronic states in the nanotube band gap. Combined with extensive first-principle simulations, our results provide direct evidence that these states originate from correlated chemisorption of hydrogen adatoms on the tube surface. The energy splitting of the paired states is governed by the adatom–adatom interaction, so that controlled hydrogenation can be used for engineering the local electronic structure of nanotubes and other sp^2-bonded nanocarbon systems.

[4] Author to whom any correspondence should be addressed.

IOP Institute of Physics ⬦ DEUTSCHE PHYSIKALISCHE GESELLSCHAFT

Contents

1. Introduction

Tailoring electronic properties of materials via doping has always been a powerful tool in device design with the most spectacular success being in silicon-based microelectronics. After the discovery of nanostructured carbon materials such as fullerenes [1], nanotubes [2], nanodiamonds [3], and the recent ability to isolate a single monolayer of graphene [4], the efficient nanoscale control over the local electronic properties of carbon materials has become increasingly important, as nanocarbon is a possible candidate to replace silicon in electronics [5].

Recent studies have attempted to dope nanocarbon with B and/or N atoms, [3], [6]–[8] and references therein. Considerable attention has also been given to effects of hydrogenation on the electronic structure of nanocarbon [9]–[13]. A single hydrogen atom chemisorbed on the wall of a sp^2-hybridized carbon system can be regarded as a defect, switching a single carbon atom from a sp^2- to a sp^3-bonding configuration and localizing the corresponding π-electron in a σ-bond. The importance of the H–C complex to control the electronic structure can be understood from organic chemistry, where the increasing degree of hydrogenation of a metallic sp^1 carbon chain changes its nature to a semiconductor (polyacetylene) or even an insulator (polyethylene).

In this work, by combining low temperature scanning tunneling microscopy and spectroscopy (LT-STM/STS) with first-principle computer simulations, we study the effects of individual adsorbed hydrogen atoms on the electronic structure of single-walled carbon nanotubes (SWNTs), which are one of the most promising members of the nanocarbon family from the viewpoint of applications in nanoelectronics. We show that one can create stable H adatoms by exposure of SWNTs to a hydrogen electron cyclotron-resonance (ECR) plasma and that these defects locally modify the electronic structure of SWNTs in a unique way. In addition to being of broad scientific interest, the study of defects in semiconductors is of prime technological importance [14]. Local carrier lifetime engineering in high power PIN silicon diodes by ion-implantation and creation of deep levels may be given here as an example [15]. In this paper, we show both experimentally and theoretically that local creation of such deep levels

IOP Institute of Physics Φ DEUTSCHE PHYSIKALISCHE GESELLSCHAFT

is also possible for semiconducting SWNTs. This ability might be used for carrier lifetime engineering in SWNT in analogy to silicon devices.

Previous experiments [16]–[20] have demonstrated that hydrogen adatoms chemisorbed onto sp^2-carbon are stable and that interaction between H adatoms lowers the adsorption energies, resulting in adatom clustering. However, the electronic structure near adatoms and effects of adatom–adatom interactions have never been experimentally studied.

2. Experimental

2.1. LT-STM/STS set-up

To get insight into the details of atomic hydrogen interaction with carbon nanotubes, we perform LT-STM/STS studies of semiconducting SWNTs subjected to hydrogen plasma treatment. The experiments were performed in a commercial LT-STM set-up (Omicron) working in ultra high vacuum (UHV) with a base pressure below 10^{-10} mbar. The STM topography images were recorded in the constant current mode with the set-point voltage applied to the sample. We used cut Pt/Ir tips for the topographic scans and the spectroscopy, where the metallic nature of the tips was checked regularly on the gold substrate.

2.2. Sample

2.2.1. Gold surface and SWNT deposition. We used HiPCo SWNTs [21] deposited on gold substrates. The SWNT raw material was sonicated for about 3 h in 1,2-dichloroethane in order to obtain a homogeneous colloidal suspension. The gold on glass substrates were treated under UHV conditions using sputtering and annealing cycles to show flat monoatomic Au(111) terraces. After *ex situ* deposition of a SWNT suspension droplet on the well-prepared gold surface with a glass pipette, we performed an additional heating cycle ($\sim$350°C) of the sample in the preparation chamber in order to remove any residue from the solvent of the suspension. STM investigation of the pristine samples revealed individual and bundled-up SWNTs, and typical herringbone structures of the Au(111) surface could still be observed on parts of the sample.

2.2.2. Creation of hydrogen plasma-induced defects. The defects on the SWNTs were created with a 2.45 GHz ECR hydrogen plasma source fitted to the preparation chamber of the LT-STM. Typical treatments with the *in situ* 2.45 GHz ECR plasma source were performed at a hydrogen pressure of about 8×10^{-2} mbar and a microwave power of 60 W. The H-ion kinetic energy distribution measured with an electrostatic analyser showed that 85% of the hydrogen ions have energy between 0 and 2 eV, and the maximum detected energy was about 16 eV. A typical ion flux with the sample positioned right under the antenna was of the order of 2×10^{13} s^{-1} cm^{-2} [16]. The sample is positioned at a vertical distance of 6 cm below the glow zone of the plasma. Further the sample can be translated horizontally up to 7 cm away from the center of the plasma glow zone, such that the ion flux on the sample can be changed by plasma power and horizontal position of the sample. A mean defect separation of about 10 nm (about 1 defect per 200 nm for intrinsic defects) is well suited to study the long-range modification of the local density of states (LDOS) induced by individual defects. Typical exposition times and position of the sample for a mean created defect separation of about 10 nm were determined
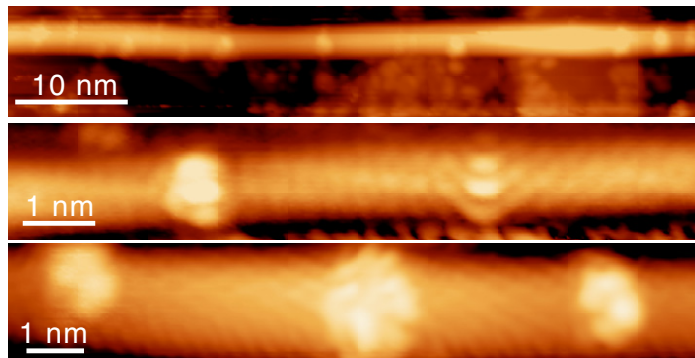
Figure 1. STM topography images of SWNTs deposited on a Au(111) surface, with hydrogen plasma-induced defects forming hillock-like protrusions with apparent heights comprised between 1 and 3 Å. Typical measurement parameters are $U_s = 1$ V, $I_s = 0.1$ nA.

with STM investigation on plasma subjected highly oriented pyrolytic graphite (HOPG). These parameters were found to be 1 s and 4.5 cm, respectively.

2.3. Topography measurements

After exposure of the SWNTs to the hydrogen plasma, STM revealed the appearance of hillock-like protrusions with apparent heights usually comprised between 1 and 3 Å and lateral extension varying between 5 Å and 20 Å, see figure 1 and the upper panels in figure 2 (all the STM topography images presented in this work were treated with the software WSXM [22], i.e. correction of the tilt plane by a plane fit if necessary and an optimization of the height scale range of the image). These hillocks could be associated with hydrogen adatoms or other point defects such as vacancies [23] and vacancy–hydrogen complexes [24]. Previous works on graphite with the same plasma conditions [17, 25] showed the occurrence of adatoms to be four times higher than that of vacancies. One can expect even more chemisorption sites on SWNTs because of the curvature-induced lowering of the adsorption energy barrier [16, 26]. Due to the fact that atomic resolution is lost at the hillocks, it was not possible to determine whether the hillocks originate from individual point defects or several close structures.

2.4. Spectroscopy measurements

The electronic structure of the hydrogen plasma-induced defects was investigated via STS using the lock-in technique. In comparison with the unperturbed regions of the SWNTs, single point spectroscopy measurements on defect sites revealed dramatic changes in the dI/dV spectra, which can be associated with changes in the LDOS [27, 28]. We have investigated a large number of defects and present here the typical cases. As the most common feature, one or two intense and very narrow peaks in the band gap were observed, see figure 2. The single peaks can be found at different positions in the bandgap, either in the midgap region or close to (or even at) the valence or conduction band edges (VBE, CBE). A pair of peaks positioned symmetrically relative to the band gap edges represents the most commonly observed feature.

To study the spatial evolution of the defect-induced modifications of the LDOS, we performed dI/dV spectra as a function of tip position x along the tube axis with a spatial
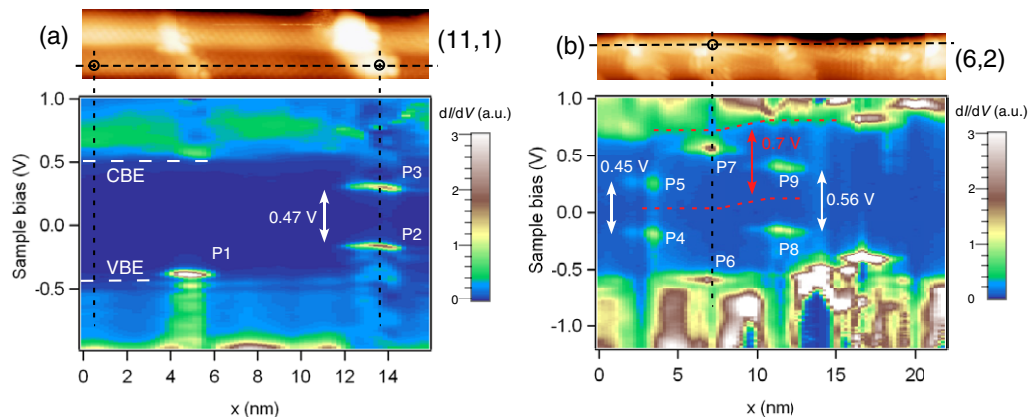
Figure 2. STM topography images of SWNTs treated with low-energy hydrogen plasma on a gold (111) substrate and the corresponding dI/dV color-scale contour maps (lower panels) for two nanotubes. The spectra were recorded along the dashed horizontal lines. A sharp single peak (P1) at the VBE and a pair of peaks (P2–P3) positioned symmetrically relative to the bandgap edges are visible in (a). FWHM of P1, P2 and P3 are 28, 26 and 33 meV, respectively. (b) Shows three defect-induced symmetric double peak structures with different energy separations. FWHM of P4, P5, P6, P7, P8 and P9 are 93, 125, 79, 84, 67 and 73 meV, respectively. Measurement parameters in (a): $U_s = 1$ V, $I_s = 0.6$ nA, $T = 5.56$ K, $U_{mod} = 6$ mV, $x_{res} = 0.21$ nm; (b): $U_s = 1$ V, $I_s = 0.3$ nA, $T = 5.36$ K, $U_{mod} = 10$ mV and $x_{res} = 0.22$ nm.

resolution of about 0.2 nm. Figures 2(a) and (b) show the dI/dV map of two semiconducting SWNTs with a series of defect sites, recorded along the horizontal dashed lines. By comparing the experimentally determined chiral angles (corrected for tip–tube convolution effects according to [29]) and the experimental bandgap energies with values from tight-binding calculations (taking into account curvature effects) [30], we could determine the chiral vectors of the semiconducting SWNTs in figures 2(a) and (b) to be (11,1) and (6,2), respectively. Note that the topography image in figure 2(a) shows a double tip artifact. The same tube is imaged here twice as we can judge from the atomic resolution where both tubes show the same chirality and also from the fact that the relative position of the two defects is the same. We have performed a number of spectroscopy line scans in this image and on both tubes the spectroscopy shows identical features. As it is actually the same tube imaged with two different protrusions of the tip, this indicates that the spectroscopic features are indeed intrinsic to the tube and not to the tip.

P1 in figure 2(a) denotes a characteristic single peak in the LDOS associated with a defect site. In the case presented here, P1 lies slightly above the VBE. The intensity of such peaks is typically about four times higher than the averaged intensity of the surrounding LDOS structure at the same position x (see figures 2(b) and (c)). On the right-hand side of figure 1(a), the frequent double peak structure mentioned above can be observed (P2–P3), with an energy separation of 0.47 eV. This energy separation of about half an electronvolt is very typical, as can be observed in analogous features (P4–P5 and P8–P9) in figure 2(b). However, larger energy separations can also occur, as P6–P7 in figure 2(b) shows, where we measure an energy difference of 1.15 eV. For each measured spectra, the STS parameters used give an

energy resolution of about $\Delta E = 15$ meV, which is about two times smaller than the narrowest measured FWHM of 26 meV for P2 in figure 1. The same spectra map of figure 2(b) shows a rigid shift of the band edges towards higher energy. A profile of the gold substrate along a line parallel to the tube axis (not shown) shows that the (6,2) tube is suspended between a terrace edge at the position $x \approx 9$ nm and another SWNT crossing at the position $x \approx 19$ nm, inducing an inhomogeneous charge transfer between the SWNT and the substrate [31]. A similar behavior was already observed for crossed SWNTs on gold and was attributed to an effective hole doping in the suspended region, resulting from a reduced screening of the charge accumulation layer by the gold substrate [31, 32].

The band shift is highlighted by the dashed red lines denoting the CBE and the midgap level, respectively. As can be clearly seen, the energetic positions of the two double peak structures P4–P5 and P8–P9 are symmetric with respect to the SWNT midgap level and not the Fermi energy from which we can deduce that they are intrinsic to the electronic structure of the modified tube and do not result from interaction with the substrate. The small spatial extent of the new electronic states below 2 nm indicates the effectiveness of our method to produce very localized and intense modifications of the electronic structure of SWNTs, yet without excessively damaging their structure. Both features, the strong modification of the electronic structure and the relatively low structural damage, are prerequisites from the perspective of using these methods to specifically alter the transport properties in SWNT-based devices.

Figures 3(a)–(c) show dI/dV plots versus bias voltage at the positions indicated by small circles for the (11,1) and (6,2) SWNTs shown in figure 2. We have characterized a large number of peak structures and found FWHMs generally between 25 and 90 meV. A maximum value of 125 meV was measured for P5 in figure 2. Figures 3(d) and (e) show details of the peaks P2 and P7 fitted with a Lorentzian function. The measured FWHMs are 26 and 84 meV. The relatively small values of the FWHM indicate that the hydrogen plasma-induced new states have a very low dispersion.

3. Density-functional theory (DFT) simulations

3.1. Simulation set-up

To understand the nature of the created defects and the type of the induced electronic modifications, we calculated the atomic and electronic structure of nanotubes with different defect structures within the framework of DFT. We used projector augmented wave (PAW) potentials [33] to describe the core electrons and the generalized gradient approximation (GGA) [34] for exchange and correlation implemented in the plane-wave code VASP [35]. All structures were fully relaxed until the forces acting on atoms were less than 0.02 eV Å^{-1}. A kinetic energy cutoff of 400 eV was found to converge the total energy of our system to within meV. The same accuracy was also achieved with respect to the **k**-point sampling of the Brillouin zone (normally 9 points along the tube axis). The band structure and LDOS were calculated with a larger number of **k**-points (32–48 points), while the electron density was kept fixed. The calculated STS spectra represent LDOS on atoms within the range of 3 Å from the adatoms averaged with equal weights.

We considered (10,0), (8,4) and (8,0) nanotubes with up to 120 carbon atoms in the simulation cell. We could not simulate the nanotubes with the chiral indices determined from the experiments due to the prohibitively large unit cells of these tubes. As our theoretical results
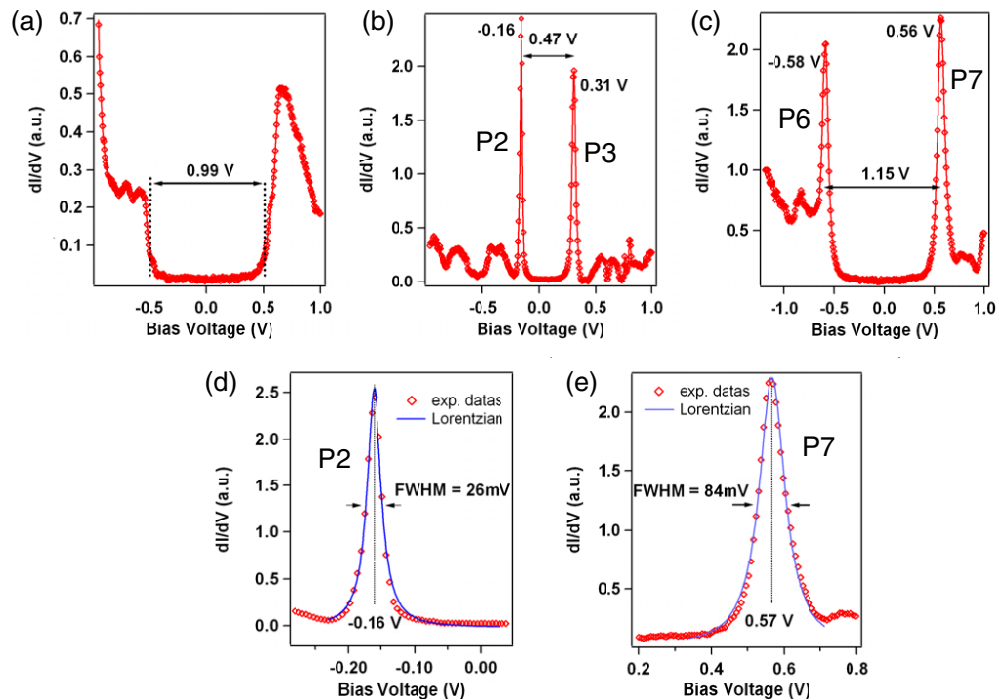
Figure 3. Comparison of spectroscopic signatures of individual point defects. dI/dV plots correspond to the positions indicated by small circles for the (11,1) SWNT shown in figure 2(a), related to the pristine nanotube (a) and the defected structure (b), respectively. (c) The same for the (6,2) SWNT, figure 2(b). P2 and P7 peaks fitted with a Lorentzian function, (d) and (e), respectively.

for the investigated tubes are in qualitative agreement with the experimental observations, we believe that our simulations for the three tubes are sufficient to generalize our results to all semiconducting SWNTs.

3.2. SWNT with a single H adatom

We started by calculating the atomic and electronic structure of nanotubes with a single H adatom. In agreement with previous simulations [9, 10, 18, 36, 37], we found that the adatom occupies the position on top of a carbon atom, figure 4(a), with adsorption energy of 1.5–2 eV and C–H bond length 1.1 Å for the tubes studied. The H adsorption energy is higher for nanotubes with small diameters than for graphene as curvature enhances sp^3 bonding. The adsorption resulted in the formation of a new dispersionless state in the middle of the gap, figure 4(d), and spatial oscillations of the electron density near the Fermi level, as shown in figure 4(b). Such oscillations near point defects were already reported for vacancies in simulations [23] and STM investigations on ion-irradiated multi-walled carbon nanotubes (MWNTs) [38], and could be assigned as $\sqrt{3} \times \sqrt{3} R30°$ superstructures due to large momentum scattering of the π-electrons at defect sites. The same characteristic superstructures can also be observed in the vicinity of hydrogen plasma-induced defects [39], indicating the possibility to tune the electronic transport properties using hydrogen adatoms.

We also studied the electronic structure of nanotubes with point defects such as single vacancies and vacancies decorated with several H atoms. We found that vacancy-related defects
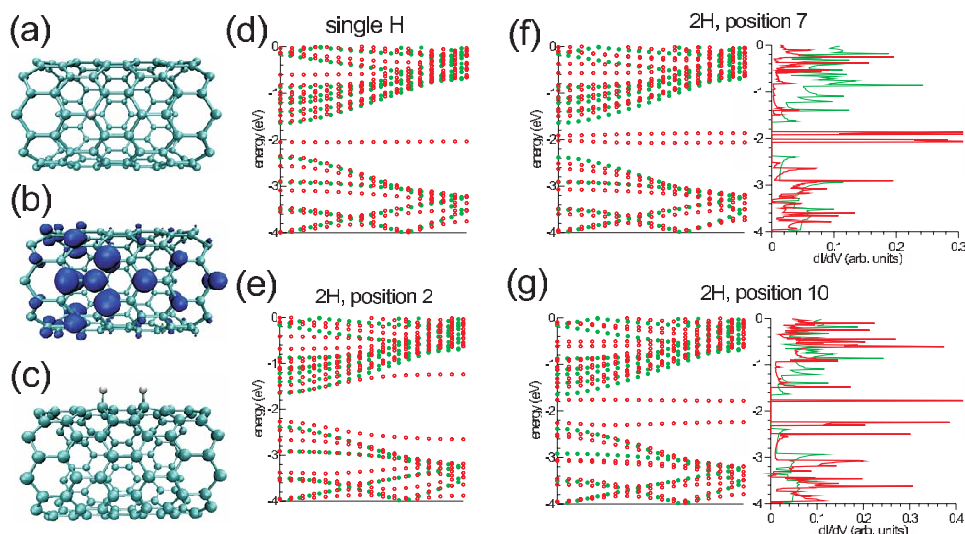
Figure 4. Electron densities and band structures for a (10,0) nanotube with one and two H adatoms. (a) Atomic structure with a single H adatom, top view. Electron density near the Fermi level (energy interval 0.7 eV) is shown in (b) for the same tube. (c) (10,0) nanotube with two nearby adatoms, side view. (d) Band structure of a nanotube with single adatom and (e) two adatoms in positions (see figure 5) 0 and 2. (f) Band structure and LDOS near two H adatoms in positions 0 and 7. (g) The same for two H adatoms in positions 0 and 10.

also result in the formation of a single peak in the gap with the peak position being dependent on the defect type. As discussed above, the probability for vacancy-type defects to appear is much smaller than for adatoms, so the H-adatoms are the most probable candidates to explain single peaks in the middle of the gap, while vacancy-H complexes may be the origin of anti-symmetric peaks, as peak P1 in figure 2 (a). None of the simulated vacancy-related defects gave rise to two peaks in the gap.

3.3. Adatom–adatom interactions

Having studied the adsorption of one H atom, we calculated the total energy and the electronic structure of nanotubes with two adatoms, as shown in figure 4(c). The different positions of the adatoms are schematically shown in figure 5(a). The first H adatom is fixed on the position labeled '0' while the second is positioned above nearby atoms as shown in figure 5(a). The total energy of the system as a function of separation between the adatoms is presented in figure 5(b). Zero energy corresponds to infinite separation of adatoms. The lowest energy configuration was found to be two adatoms on adjacent sites.

It is evident from figure 5 that the energy depends non-monotonously on the adatom separation, with the minima at the sites corresponding to the cusps in the electron density near a single adatom, cf figures 5(a) and 4(b). The difference in energies corresponding to different adsorption positions was more than 1 eV at small separations (positions '0–2' and '0–4', in agreement with the results for graphite [19, 20]). The difference clearly originates from electronic effects, as (i) H adatoms do not give rise to a large distortion of the lattice, so that interaction through strain fields can be excluded; (ii) the maxima–minima structure perfectly
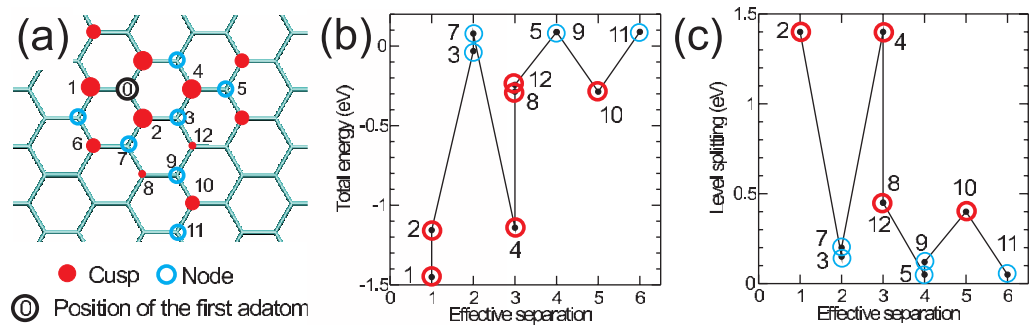
Figure 5. First-principles simulations for a (10,0) SWNT with H adatoms. (a) The adsorption sites of H adatoms. All positions are metastable (separated by energy barriers from each other) so that all of them can exist at low experimental temperatures. The red and blue circles reflect the nodal structure of electron density oscillation near the Fermi energy when there is a single adatom on site labeled '0'. (b) The total energy of the system for different positions of the second adatom. The separation between adatoms is defined as the number of bonds in graphene lattice on the migration path of the second adatom to arrive at site '0'. (c) The splitting of the H-induced levels in the gap due to adatom–adatom interaction.

matches the cusp–node pattern in the electron density near a single adatom. The saw-tooth dependence can be understood in terms of the slightly different amount of π-electron density available near the Fermi level for making a bond between the nanotube atom and the second H adatom.

A similar phenomenon—substrate mediated long-ranged oscillatory interaction—was previously reported for adatoms on metal surfaces [40]. However, such a result is somewhat unexpected for a semiconducting system, as the new states should be more spatially localized near the defect than in a metal system. Although the simulated nanotubes were too small to quantitatively extrapolate the dependence to large adatom separation, one can assume from tight-binding simulations for bigger systems [23] that the interaction is effective in a range of up to dozen nanometres, coinciding with the extension of electronic superstructures near the defects.

Adatom–adatom interaction gives rise to another salient feature: the H adatom-induced states split into two peaks in the LDOS which are symmetric with the midgap level, as shown in figures 4(e)–(g). Depending on the adatom–adatom separation, the position of the peaks can be in the middle of the gap (deep levels), figure 4(f), close to the band edges (shallow levels), figure 4(g), or at the band edges, figure 4(e). All these positions were found to be metastable (separated by energy barriers from each other) so that all of them can exist at the experimental temperature of about 5 K. The structures presented in (f) and (g), with a maximum peak FWHM of 60 meV are in very good agreement with the measurements, and can be associated with the double peak spectra P2–P3, P4–P5, P8–P9 (deep levels) and P6–P7 (shallow levels) presented in figure 2. An important feature can be seen in figure 5(c): the splitting is proportional to the adsorption energy for the second adatom and thus to the strength of the adatom–adatom interaction.

IOP Institute of Physics ⏀ DEUTSCHE PHYSIKALISCHE GESELLSCHAFT

4. Conclusions and outlook

Our results indicate that H adatom adsorption energy is different if there is another adatom nearby, with the interaction being non-monotonously dependent on the separation. As adatom–adatom interaction changes the sticking coefficients for H on graphite [20], this is also likely to happen in SWNTs, thus explaining the abundance of double-peak structures. The interaction should also affect adatom diffusion[5] and hydrogen desorption (e.g. due to additional barriers for diffusion from site '4' to site '0' via site '3'), and assuming that the chemisorption mechanism is more important than molecular physisorption [41], thus maximum hydrogen uptake in nanotubes. Note that this effect is not taken into account in numerous Monte-Carlo simulations of hydrogen–nanotube interactions.

The interplay between sticking, desorption and diffusion can be used to control the distribution of H–H adatoms. Thus our results point out that partial hydrogenation of carbon nanotubes by using, e.g. masks, followed by annealing at pre-determined temperatures can be employed for engineering the electronic structure of nanotubes and creating paired states in the semiconducting gap. This has important implications in, for example, optoelectronics [42] where the symmetric gap states can act as local recombination centers for electrons and holes by emission of a photon of well-defined energy. Formation of new states can also be expected in graphene nanoribbons and other graphitic systems. The changes in the electronic structure due to long-ranged interactions between adatoms may also be very important for understanding proton-irradiation-induced magnetism in carbon systems [43]–[45].

To conclude, we used hydrogen-plasma treatment and LT-STM/STS methods to alter the electronic structure of semiconducting nanotubes. Our experiments and first-principles simulations provide direct evidence for the correlated chemisorption of hydrogen adatoms on the nanotube surface, clearly manifested by new states in the band gap. As the positions of the new states are governed by the adatom–adatom distribution, controlled hydrogenation can be used for engineering the local electronic structure of carbon nanotubes.

---

[5] The desorption barrier for the H adatom on graphite is slightly lower than the diffusion barrier [20], implying that the adatom will desorb rather than diffuse upon heating. At the same time, it is well known that nanotube curvature increases the adsorption energies [16, 26] and makes the diffusion of adatoms and other defects [46, 47] anisotropic. Although one may expect that the barriers for diffusion perpendicular to the tube axis will increase, the diffusion parallel to the tube axis should be roughly the same as in graphite. Thus, the diffusion mechanism for adatoms on nanotubes should be active and could explain the abundance of dimers with low hydrogen irradiation doses. The detailed study of H adatom diffusion on nanotubes is beyond the scope of this work.

IOP Institute of Physics **Φ** DEUTSCHE PHYSIKALISCHE GESELLSCHAFT

References

[1] Kroto H W, Heath J R, O'Brien S C, Curl R F and Smalley R E 1985 C$_{60}$: buckminsterfullerene *Nature* **318** 162–3

[2] Iijima S 1991 Helical microtubules of graphitic carbon *Nature* **354** 56–8

[3] Talapatra S, Ganesan P G, Kim T, Vajtai R, Huang M, Shima M, Ramanath G, Srivastava D, Deevi S C and Ajayan P M 2005 Irradiation-induced magnetism in carbon nanostructures *Phys. Rev. Lett.* **95** 097201

[4] Novoselov K S, Geim A K, Morozov S V, Jiang D, Katsnelson M I, Grigorieva I V, Dubonos S V and Firsov A A 2005 Two-dimensional gas of massless dirac fermions in graphene *Nature* **438** 197–200

[5] McEuen P L 1998 Carbon-based electronics *Nature* **393** 15–7

[6] Droppa R Jr, Ribeiro C T M, Zanatta A R, dos Santos M C and Alvarez F 2004 Comprehensive spectroscopic study of nitrogenated carbon nanotubes *Phys. Rev.* B **69** 045405

[7] Kotakoski J, Krasheninnikov A V, Ma Y, Foster A S, Nordlund K and Nieminen R M 2005 B and N ion implantation into carbon nanotubes: insight from atomistic simulations *Phys. Rev.* B **71** 205408

[8] Ewels C P and Glerup M 2005 Nitrogen doping in carbon nanotubes *J. Nanosci. Nanotechnol.* **5** 1345–63

[9] Yildirim T, Gülseren O and Ciraci S 2001 Exohydrogenated single-wall carbon nanotubes *Phys. Rev.* B **64** 075404

[10] Lee S M, An K H, Lee Y H, Seifert G and Frauenheim T 2001 A hydrogen storage mechanism in single-walled carbon nanotubes *J. Am. Chem. Soc.* **123** 5059–63

[11] Duplock E J, Scheffler M and Lindan P J D 2004 Hallmark of perfect graphene *Phys. Rev. Lett.* **92** 225502

[12] Zhang G, Qi P, Wang X, Lu Y, Mann D, Li X and Dai H 2006 Hydrogenation and hydrocarbonation and etching of single-walled carbon nanotubes *J. Am. Chem. Soc.* **128** 6026–7

[13] Barnard A S, Russo S P and Snook I K 2003 Electronic band gaps of diamond nanowires *Phys. Rev.* B **68** 235407

[14] Stavola M 1999 To 40 years of defects in semiconductors: may the problem never be solved! *Physica* B **273–4** 1–6

[15] Vobecký J and Hazdra P 2002 High-power P-i-N diode with the local lifetime control based on the proximity gettering of platinum *IEEE Electron Device Lett.* **23** 392

[16] Ruffieux P, Gröning O, Bielmann M, Mauron P, Schlapbach L and Gröning P 2002 Hydrogen adsorption on sp^2-bonded carbon: influence of the local curvature *Phys. Rev.* B **66** 245416

[17] Ruffieux P, Gröning O, Schwaller P, Schlapbach L and Gröning P 2000 Hydrogen atoms cause long-range electronic effects on graphite *Phys. Rev. Lett.* **84** 4910–3

[18] Allouche A, Ferro Y, Angot T, Thomas C and Layet J-M 2005 Hydrogen adsorption on graphite (0001) surface: a combined spectroscopy-density-functional-theory study *J. Chem. Phys.* **123** 124701

[19] Hornekær L, Šljivančanin Ž, Xu W, Otero R, Rauls E, Stensgaard I, Lægsgaard E, Hammer B and Besenbacher F 2006 Metastable structures and recombination pathways for atomic hydrogen on the graphite (0001) surface *Phys. Rev. Lett.* **96** 156104

[20] Hornekær L, Rauls E, Xu W, Šljivančanin Ž, Otero R, Stensgaard I, Lægsgaard E, Hammer B and Besenbacher F 2006 Clustering of chemisorbed H(D) atoms on the graphite (0001) surface due to preferential sticking *Phys. Rev. Lett.* **97** 186102

[21] Chiang I W, Brinson B E, Huang A Y, Willis P A, Bronikowski M J, Margrave J L, Smalley R E and Hauge R H 2001 Purification and characterization of single-wall carbon nanotubes (SWNTs) obtained from the gas-phase decomposition of CO (HiPco process) *J. Phys. Chem.* B **105** 8297–301

[22] Horcas I, Fernandez R, Gomez-Rodriguez J M, Colchero J, Gomez-Herrero J and Baro A M 2007 WSXM: A software for scanning probe microscopy and a tool for nanotechnology *Rev. Sci. Instrum.* **78** 013705

[23] Krasheninnikov A V 2001 Predicted scanning microscopy images of carbon nanotubes with atomic vacancies *Sol. Stat. Commun.* **118** 361–5

[24] Hjort M and Stafström S 2000 Modeling vacancies in graphite via the Hückel method *Phys. Rev.* B **61** 14089–94

[25] Ruffieuxt P, Melle-Franco M, Gröning O, Bielmann M, Zerbetto and Gröning 2005 Charge-density oscillation on graphite induced by the interference of electron waves *Phys. Rev.* B **71** 153403

[26] Park S, Srivastava D and Cho K 2003 Generalized chemical reactivity of curved surfaces: carbon nanotubes *Nano Lett.* **3** 1273–7

[27] Tersoff J and Hamann D R 1985 Theory of the scanning tunneling microscope *Phys. Rev.* B **31** 805–13

[28] Hofer W, Foster A S and Shluger A L 2003 Theories of scanning probe microscopes at the atomic scale *Rev. Mod. Phys.* **75** 1287–331

[29] Venema L C, Meunier V, Lambin Ph and Dekker C 2000 Atomic structure of carbon nanotubes from scanning-tunneling microscopy *Phys. Rev.* B **61** 2991–6

[30] Yorikawa H and Muramatsu S 1995 Energy gaps of semiconducting nanotubules *Phys. Rev.* B **52** 2723–7

[31] Janssen J W, Lemay S G, Kouwenhoven L P and Dekker C 2002 Scanning tunneling spectroscopy on crossed carbon nanotubes *Phys. Rev.* B **65** 115423

[32] Vitali L, Burghard M, Wahl P, Schneide M A and Kern K 2006 Local pressure-induced metallization of a semiconducting carbon nanotube in a crossed junction *Phys. Rev. Lett.* **96** 086804

[33] Blöchl P E 1994 Projector augmented-wave method *Phys. Rev.* B **50** 17953–79

[34] Perdew J P, Chevary J A, Vosko S H, Jackson K A, Pederson M R, Singh D J and Fiolhais C 1992 Atoms, molecules, solids and surfaces: applications of the generalized gradient approximation for exchange and correlation *Phys. Rev.* B **46** 6671–87

[35] Kresse G and Furthmüller J 1996 Efficient iterative schemes for *ab initio* total-energy calculations using a plane-wave basis set *Phys. Rev.* B **54** 11169–86

[36] Ferro Y, Marinelli F and Allouche A 2003 Density functional theory investigation of the diffusion and recombination of H on a graphite surface *Chem. Phys. Lett.* **368** 609–15

[37] Barnard A S, Terranova M L and Rossi M 2005 Density functional theory of H-induced defects as nucleation sites in hybrid carbon nanomaterials *Chem. Mater.* **17** 527–35

[38] Osváth Z, Vértesy G, Tapasztó L, Wéber F, Horváth Z E, Gyulai J and Biró L P 2005 Atomically resolved STM images of carbon nanotube defects produced by Ar$^+$ irradiation *Phys. Rev.* B **72** 045429

[39] Buchs G, Ruffieux P, Gröning P and Gröning O 2007 Scanning tunneling microscopy investigations of hydrogen plasma induced electron scattering centers on single-walled carbon nanotubes *Appl. Phys. Lett.* **90** 013104

[40] Repp J, Moresco F, Meyer G and Rieder K-H 2000 Substrate mediated long-range oscillatory interaction between adatoms: Cu/Cu(111) *Phys. Rev. Lett.* **85** 2981–4

[41] Nikitin A, Ogasawara H, Mann D, Denecke R, Zhang Z, Dai H, Cho K and Nilsson A 2005 Hydrogenation of single-walled carbon nanotubes *Phys. Rev. Lett.* **95** 225507

[42] Iakoubovskii K, Minami N, Kim Y, Miyashita K, Kazaoui S and Nalini B 2006 Midgap luminescence centers in single-wall carbon nanotubes created by ultraviolet illumination *Appl. Phys. Lett.* **89** 173108

[43] Esquinazi P, Spearmann D, Höhne R, Setzer A and Butz T 2003 Induced magnetic ordering by proton irradiation in graphite *Phys. Rev. Lett.* **91** 227201

[44] Chan J A, Montanari B, Gale J D, Bennington S M, Taylor J W and Harrison N M 2004 Magnetic properties of polymerized C_{60}: the influence of defects and hydrogen *Phys. Rev.* B **70** 041403(R)

[45] Lehtinen P O, Foster A S, Ma Y, Krasheninnikov A V and Nieminen R M 2004 Irradiation-induced magnetism in graphite: a density functional study *Phys. Rev. Lett.* **93** 187202

[46] Krasheninnikov A V, Nordlund K, Lehtinen P O, Foster A S, Ayuela A and Nieminen R M 2004 Adsorption and migration of carbon adatoms on carbon nanotubes: density functional *ab initio* and tight-binding studies *Phys. Rev.* B **69** 073402

[47] Krasheninnikov A V, Lehtinen P O, Foster A S and Nieminen R M 2006 Bending the rules: contrasting vacancy energetics and migration in graphite and carbon nanotubes *Chem. Phys. Lett.* **418** 132